Tectonophysics 657 (2015) 102–112

Contents lists available at ScienceDirect

Tectonophysics

journal homepage: www.elsevier.com/locate/tecto

The flat to normal subduction transition study to obtain the Nazca plate morphology using high resolution seismicity data from the Nazca plate in Central Chile

Silvina Nacif [a,*], Enrique G. Triep [a], Silvana L. Spagnotto [b,c], Eugenio Aragon [d], Renzo Furlani [a], Orlando Álvarez [a,b]

[a] Instituto Geofísico Sismológico F. Volponi, Universidad Nacional de San Juan, Ruta 12, km 17, Marquesado, Rivadavia, San Juan, Argentina
[b] Consejo Nacional de Investigaciones Científicas y Técnicas, Conicet, Argentina
[c] Departamento de Física, Universidad Nacional de San Luis, Ejército de los Andes 950, 5700, San Luis Argentina
[d] Centro de Investigaciones Geológicas, Universidad Nacional de la Plata, Calle 1N° 644, Argentina

ARTICLE INFO

Article history:
Received 23 October 2014
Received in revised form 17 June 2015
Accepted 24 June 2015
Available online 9 July 2015

Keywords:
Intraslab-depth earthquakes
Subduction zones
Subducted slab morphology
Dehydration process

ABSTRACT

Data from 45 seismological stations mostly temporary were used to obtain an accurate data set of intraslab seismicity of the Nazca subducted plate between 33°S and 35°S. The interest zone located in the transition section where the Nazca plate changes from flat slab north of ~33° to normal slab south of that latitude. In addition, the study region is located where the active volcanic arc appears. From a set of earthquakes which were relocated using a grid-search multiple events algorithm we obtained the plate geometry from latitudes of 33°S to 34.5°S and from 60 km to 120 km in depth. The obtained morphology shows notable similarity in its structure to Maipo Orocline revealing some possible strong connection between the overriding plate and the subducting plate. We suggest that the subducted plate at the trench has been deformed in its shape consistently with the Maipo Orocline pattern and its deformation is observed below the interface zone. Our results are consistent with van Keken et al., 2011 models, and based on this the seismicity located between 70 and 120 km is probably related with dehydration processes rather than mechanical processes. From our precise earthquake locations we observed a complete lack of intraslab seismicity below 120 km depth. This valuable finding can be used to better constrain thermal models for the subduction region of Central Chile.

1. Introduction

A constrained geometry of the subducted plate constitutes a key role in subduction zone structure. Several research works have focused in this issue (e.g., England et al., 2004; Syracuse and Abers, 2006; Hayes and Wald, 2009; Hayes et al., 2012). Hayes et al. (2012) used 2D cross-sections in a three-dimensional interpolation scheme to produce three-dimensional geometry of ~85% of subduction zones worldwide. Knowledge of the 3D geometry is a useful feature to constrain thermal models in subduction zones that have oblique convergence (Bengston and van Keken, 2012). In addition, subduction plate structure represents essential information to complement tectonic interpretations from evidences (such as a velocity anomaly) of seismic tomography/anisotropy, receiver function, among others. Interslab events are related with underthrusting mechanisms which jointly with intraslab events (below the downdip edge) define the slab shape. Many authors have studied the seismogenic plate interface in subduction zones around the world considering that the greatest earthquakes occurred there (e.g., Ruff and Kanamori, 1983; Nishenko, 1985; Pacheco et al., 1993; Ruff and Tichelaar, 1996; Heuret et al., 2011). Heuret et al. (2011) found that the subduction velocity is a first-order parameter which controls the variability in the physical characteristics in the plate interface. Those authors determined the geometry and the mechanical behavior from a statistical research over a global study about subduction interface seismogenic zones. The slab geometry evolution has been studied by different authors (e.g., van Hunen et al., 2004; Manea and Gurnis, 2007; Manea et al., 2012). Three mechanisms, which can provide an explanation for slab flattening, were grouped and investigated by van Hunen et al. (2004): subduction of lithosphere with increased buoyancy, subduction below a trenchward moving overthrusting continent, and slab suction forces in the mantle wedge. From numerical modeling experiments, those authors concluded that a trenchward overthrusting continent easily provides the conditions for flat subduction whereas, favorable conditions for flat subduction due only to the effect of a subducting oceanic plateau are less common. Additionally, Manea and Gurnis (2007) explored the influence of low viscosity wedge and channel on subduction zone structure using numerical models. These authors concluded that the viscosity reduction and the maximum depth of the low viscosity wedge play important control in the slab dip. Reducing the

* Corresponding author. Tel.: +54 0264 4945015.
E-mail addresses: nacif.silvina@gmail.com (S. Nacif), egtriep@gmail.com (E.G. Triep), pampa113@gmail.com (S.L. Spagnotto), earagon@cig.museo.unlp.edu.ar (E. Aragon), rfurlani1@gmail.com (R. Furlani), orlando_a_p@yahoo.com.ar (O. Álvarez).

http://dx.doi.org/10.1016/j.tecto.2015.06.027
0040-1951/

wedge viscosity by half (with respect to the upper mantle viscosity) or by adding a shallow "lower viscosity wedge" (200 km), Manea and Gurnis (2007) highlighted that a perfectly flat slab could be obtained. At last, the trenchward motion of thick cratonic lithosphere with trench retreat had also been proposed to promote slab flattening (Manea et al., 2012).

The subducted Nazca plate is seismically active from the trench to depths of ~150–200 km (e.g., NEIC Catalog, Anderson, et al., 2007; Marot et al., 2014). Marot et al. (2014) studied the seismicity associated with the Nazca plate in the flat section and in the normal section (between 29°S and 35°S). Those authors observed that the normal slab (south of 33°S) down to 50 km depth is less seismogenic compared with flat section. In addition, between 50 and 75 km depth the seismic activity increases. The study zone in our research (Fig. 1) is located just above where an increase in seismicity has been observed. In Fig. 2 we show cross-sections, in which at 33.5°S and 34.5°S the intraslab seismicity is less frequent below ~130 km depths.

This paper focuses on the seismicity below the interface seismogenic zone (intermediate-depth earthquake). This intermediate-depth seismicity (50–300 km) has been related to pull slab forces, eclogitization processes due to dehydration of the slab, reactivation of normal faults created in the outer rise zone and thermally modulated ductile or shear instabilities (Raleigh and Paterson, 1965; Ogawa, 1987; Meade and Jeanloz, 1991; Kirby et al., 1996; Jiao et al., 2000; Hacker et al., 2003; Kelemen and Hirth, 2007). Laboratory experiments (Jung et al., 2004) have demonstrated that earthquakes located at intermediate depths could be originated by dehydration embrittlement accompanied by negative volume changes. Nevertheless, Barcheck et al. (2012) suggest that dehydration embrittlement cannot be the primary factor

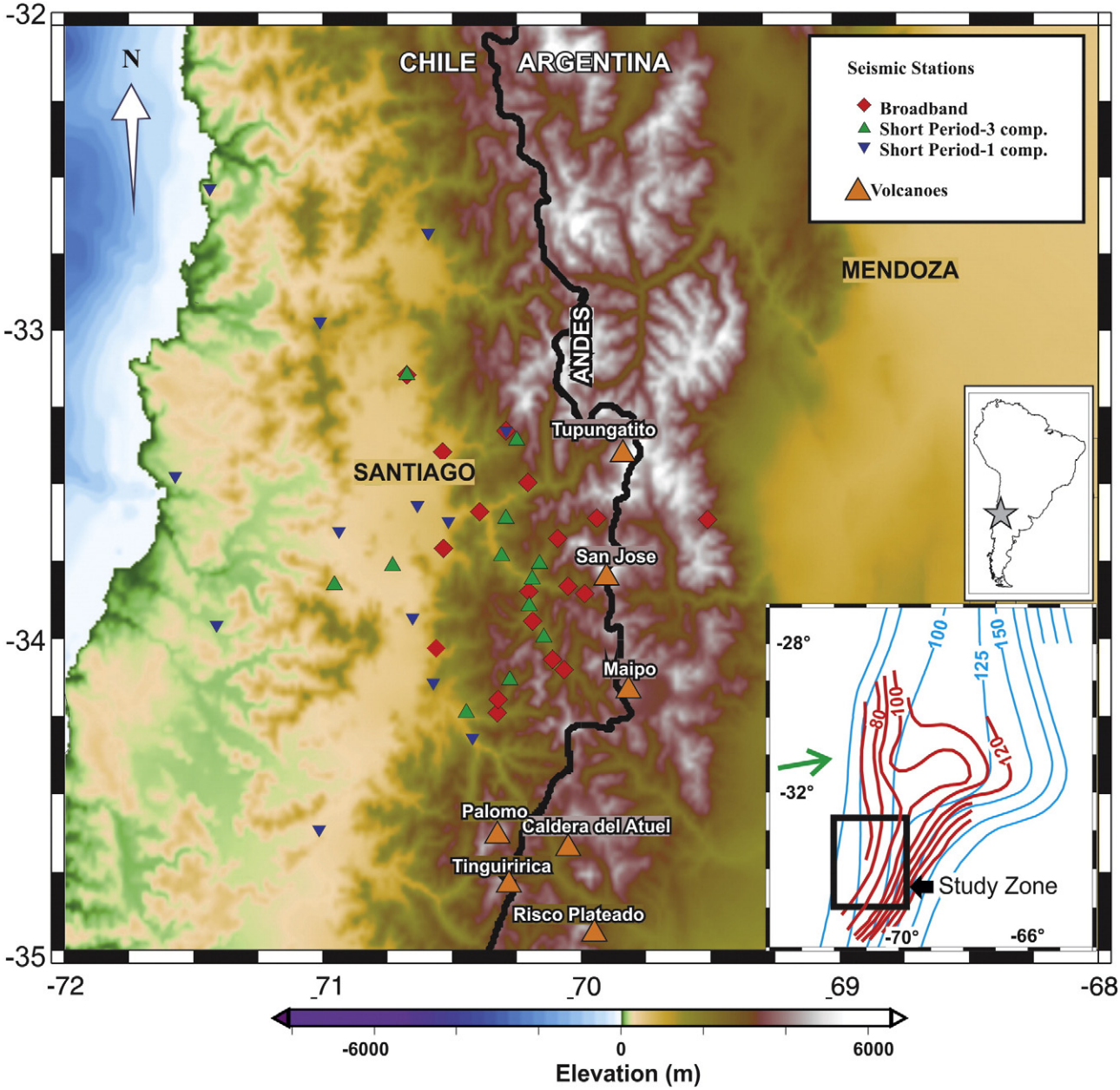

Fig. 1. Study region map which shows the deployed stations by CHASE experiment. The major stations are located in Principal Cordillera, several in Central Valley and Coastal Cordillera and only one in Frontal Cordillera in Argentina. Volcanoes are shown by orange triangles (Hildreth and Moorbath, 1988). The upper inset shows (gray star) the study region located in South America. The lower inset shows the contours of the Nazca oceanic plate by Cahill and Isacks (1992) and Anderson et al. (2007) in blue and red lines, respectively.

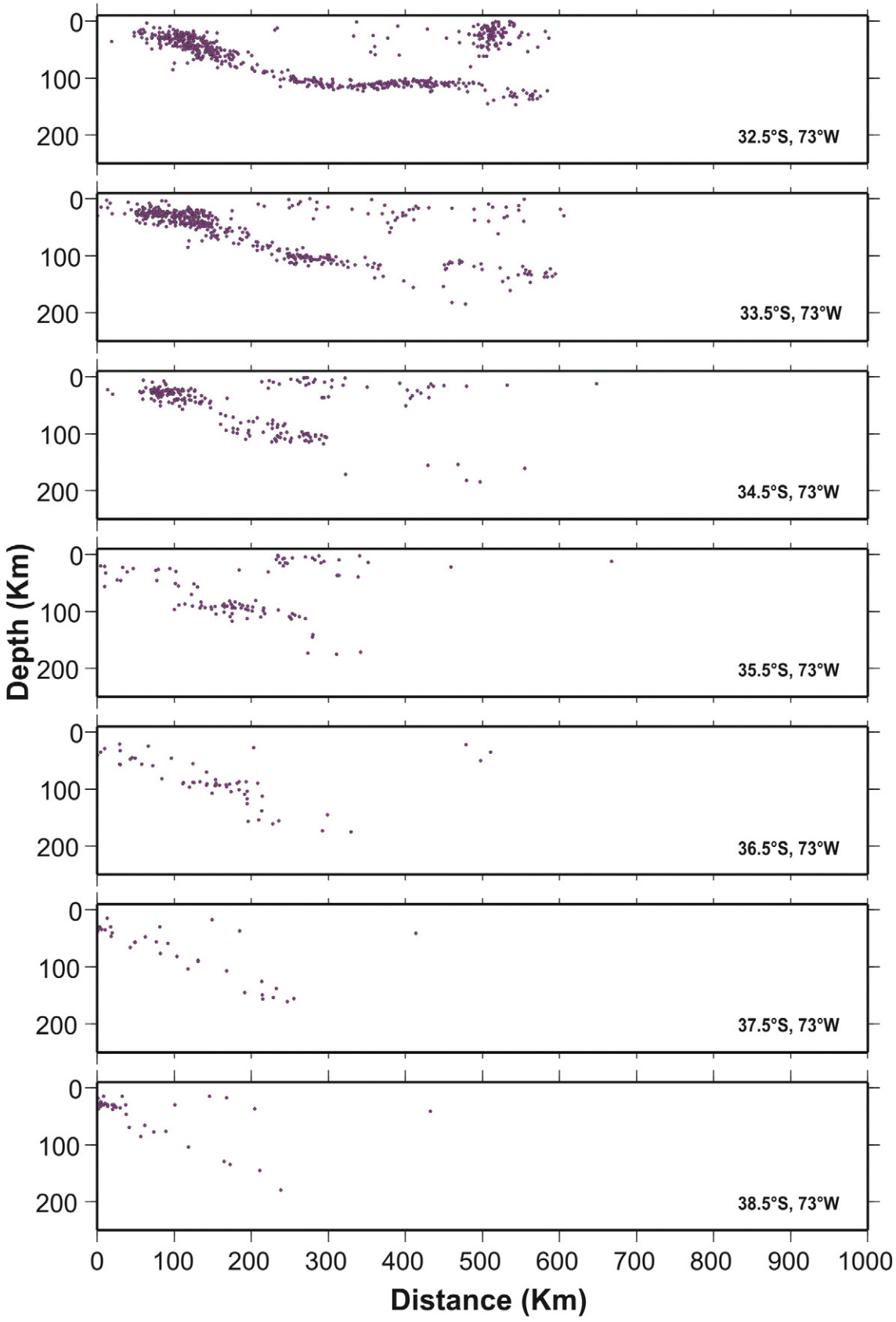

Fig. 2. Seismicity of a period of time of ~48 years (1960–2008) from International Seismological Centre, EHB Bulletin, http://www.isc.ac.uk, Internatl. Seis. Cent., Thatcham, United Kingdom, 2009. The W–E cross-sections show the hypocenters (violet points) which belong to the Nazca subducted plate, to the South American plate and to their contact. The origins of the profiles are shown by the latitude and the longitude in the lower part of each cross-section. In order to show the Nazca dip variation from north to south, the seismicity located up to 100 km on both sides of the profile is plotted in each cross-section. From north to south (top to bottom) it can be seen how the dip angle increases and the plate seismic activity decreases.

controlling the occurrence of these earthquakes. No strong correlation between dehydration flux and seismicity rate was found (depths < 240 km). As mentioned before, another mechanism which can explain those earthquakes is thermal softening (in viscoelastic material) leading to shear instabilities (Ogawa, 1987). From a theoretical study Braeck and Podladchikov (2007) quantified the conditions under which viscoelastic material fails as a result of thermal runaway. Those authors explained that at high stresses, viscous dissipation becomes substantial, and if heat is generated faster than it is conducted away, the local increase in temperature and strain rate is strongly amplified. Then, the thermal runaway is developed. The applicability of thermal runaway theory to intermediate-depth earthquakes was developed by John et al. (2009). Using fully coupled thermal and viscoelastic models, John et al. (2009) concluded that self-localizing thermal runaway is a viable mechanism for intermediate-depth earthquake in subducting slabs.

Although the morphology of the Nazca plate in central Chile is well-described by different authors (Cahill and Isacks, 1992; Araujo and Suarez, 1994; Syracuse and Abers, 2006; Anderson et al., 2007) we present a detailed structure of the Nazca plate below the seismogenic interface zone which can be used for local studies. For this seismicity we obtained precise locations and focal mechanism solutions. The dense network deployed allows us to define the precise locations of intermediate-depth earthquakes. Then, this advantage controls the constrain morphology obtained from those data. Unlike iterative lineal algorithm (such as Hypoinverse, Klein, 2002), the location technique used in this work tests the entire solution space by a direct and grid-search method. In addition, this algorithm performs the uncertainty analysis in the context of the multiple-event location problem in which the location parameters of a set of events are determined jointly with travel-time corrections associated with the paths between the events and recording stations (Rodi, 2006). This approach is essential to obtain well-resolvable hypocenter determinations.

2. Seismotectonic setting

The western South American border is characterized by a convergent margin, in which the Nazca plate subducted underneath the South American plate, by 63 mm/year of relative convergence velocity (Kendrick et al., 2003). At the study region latitudes the age of the oceanic lithosphere in the trench is ~32.4 ± 0.8 My (Syracuse and Abers, 2006) which corresponds to a thermal mature subduction zone (Kirby et al., 1996). In general, subducted slabs around the world commonly sink at steep angles. However our study region (Fig. 1) is composed of the transition section where the Nazca plate changes from flat slab north of ~33° to normal slab south of this latitude (Cahill and Isacks, 1992; Araujo and Suarez, 1994; Pardo et al., 2002; Syracuse and Abers, 2006; Anderson et al., 2007). The flat slab segments have been associated spatially and temporally with thickened oceanic crust (e.g., Gutscher et al., 2000). However, van Hunen et al. (2002) showed that the length of an occurring flat slab segment was limited to about 300 km (only in the case of a kinematic hindered reaction from basalt to eclogite). This does not apply to the surrounding study region, which flat slab extends up 500 km from the trench (see contours Nazca plate by Anderson et al., 2007). In addition, major changes of slab dynamics have been not observed by numerical experiment modeling subduction of a moderate size aseismic ridge (Gerya et al., 2009). In particular, for the Juan Fernandez Ridge, is an example where an analogue experiment (Martinod et al., 2005) shows that this ridge did not significantly alter the subduction process. A recent publication emphasized the importance of the upper plate properties in controlling the plate geometry (e.g., Manea et al., 2012). To explore how trenchward motion of thick cratons may result in Chilean flat slab, Manea et al. (2012) had designed time-dependent numerical experiments. Their results show that only the combination of trenchward motion of thick cratonic lithosphere with trench retreat is able to reproduce the temporal and spatial evolution of slab flattening and its associated upper plate deformation and volcanism.

We selected the seismicity for the study region and surrounding areas from EHB Bulletin (http://www.isc.ac.uk) since 1960–2008. From this catalog several cross-sections at different latitudes were plotted (Fig. 2). The flat section is shown in cross-section at 32.5°S, the cross-section at 33.5°S shows a normal subduction with the influence of the flat slab section, and the other profiles show a steeper subduction without disturbance of the flat section. From North to South the Nazca plate becomes less seismic in accordance with a young and hot lithosphere. South of ~33.5°S, in agreement with the change from flat to steep slab, the active Pliocene–Quaternary volcanism (Hildreth and Moorbath, 1988; Kay et al., 2005) appears. This active volcanism is composed of the Northern part of the Andean Southern Volcanic Zone, absent to the North from ~9–10 My (e.g., Kay et al., 1987). Additionally, the Andean margin at this latitude is characterized by along strike curvature known as Maipo Orocline (Yáñez et al., 2002; Farías et al., 2008).

The study of the interface seismogenic zone has been related to 1985 Mw = 8.0 Valparaiso earthquake (Christensen and Ruff, 1986; Comte et al., 1986; Barrientos, 1988; Choy and Dewey, 1988; Tichelaar and Ruff, 1991; Mendoza et al., 1994; among others), when the rupture reached a length and width of ~200 km and ~100 km, respectively. This earthquake has been the largest for the last 40 years in the region. Due to its lower environmental, intraslab earthquakes from the Nazca subducted plate have been less studied, but a well-documented earthquake (Marot et al., 2012) by a local network is 2003 Mw = 5.7 at 120 km depth within the subducting Nazca plate. The focal mechanism solution for this earthquake is normal faulting and from the aftershocks distribution, Marot et al. (2012) proposed that this earthquake is a reactivation of outer rise faults formed during flexural bulge.

3. Data and methods

Data are from Chile Argentina Seismic Experiment (CHASE) which has been registered since November 2005 to March 2006 and covered a local area from latitude 32.5°–34.75°S and longitude 69.25°–71.5°W (Fig. 1). The experiment deployed 18 broad band stations, 15 short period stations with 3 components and 12 short period stations with only one vertical component. We unified all the registers from different acquisition systems to SEISAN (Havskov et al., 2007) seismic format and created an event data base after continuous registers were observed; in this manner we maximize the number of seismic events which were found. SEISAN multitrace view was used for P and S wave arrival identification in totally 5269 P phases and 4198 S phases were read. The process explained here was done for the overriding and subducted plate seismic events, but in this work we only show results of the events from the subducted Nazca plate.

We located 412 events with a single determination code called HYPOCENTER (Liener and Havskov, 1995) using a one dimensional velocity model obtained by Nacif (2012), shown in inset of Fig. 3. Based on Maurer et al. (2010) we removed systematic errors in travel-time data due to incorrect station coordinates, errors in the acquisition time at each station and/or inconsistency in the picking due to low signal/noise level. We selected a subset from HYPOCENTER results of 322 events for relocated seismicity by GMEL (Rodi, 2006) which applies a maximum-likelihood grid-search algorithm to find location parameters within a cluster of events and solves station travel-time correction simultaneously. At the time grid-search algorithm is applied the method allows association between the set of arrivals to a particular event. Ellipticity corrections were not necessary considering the small area covered by the experiment of ~150 km × 150 km. Travel-time tables (step of 1 km and 0.01° for depth and epicentral distance) were calculated with TauP Toolkit (Crotwell and Owens, 1998) using the velocity model from Nacif (2012) from which theoretical times were extracted. As regards picking errors GMEL considered that are statistically

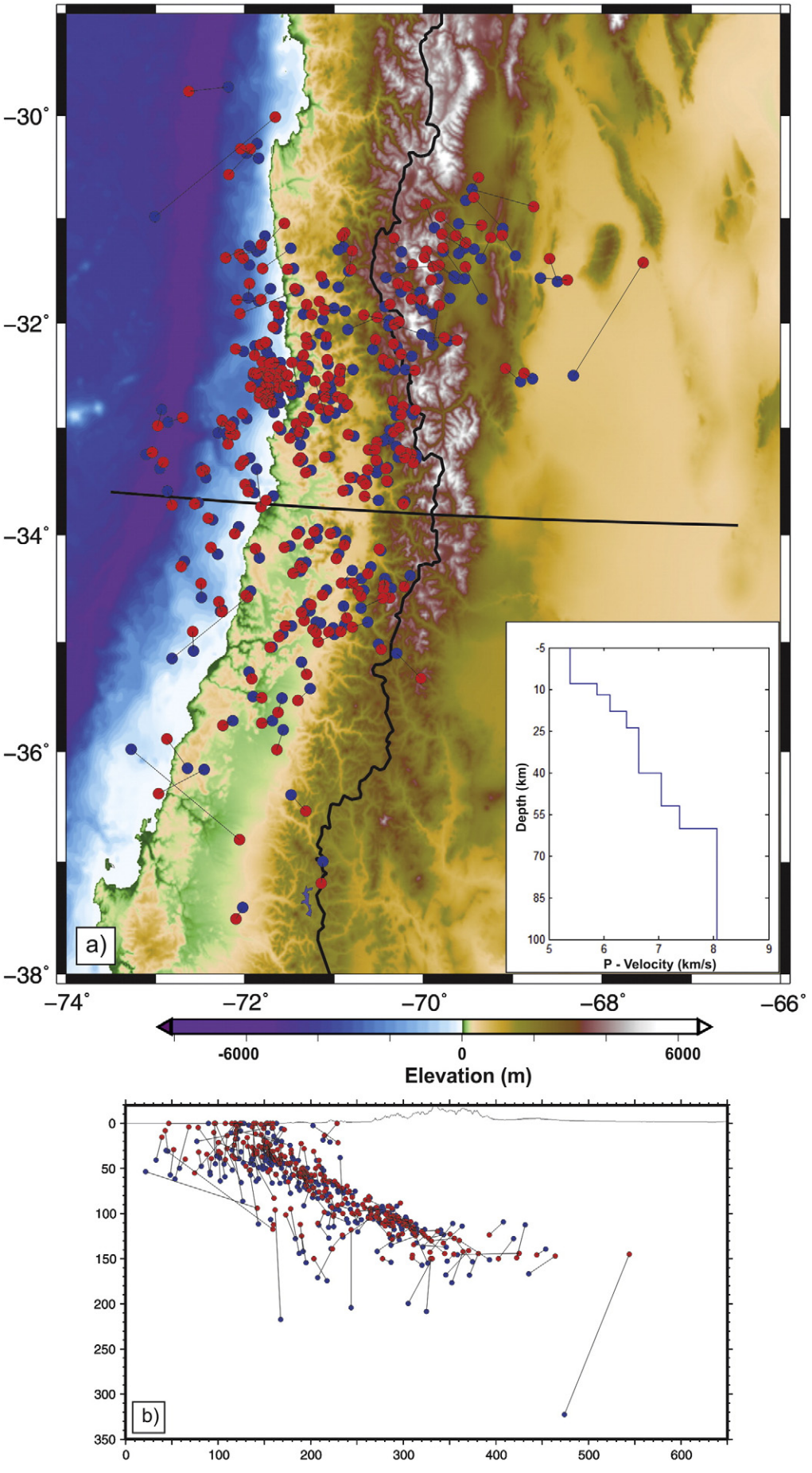
−30°
−32°
−34°
−36°
−38°
−74°
−72°
−70°
−68°
−66°
a)
Depth (km)
P - Velocity (km/s)
-6000
0
6000
Elevation (m)
b)

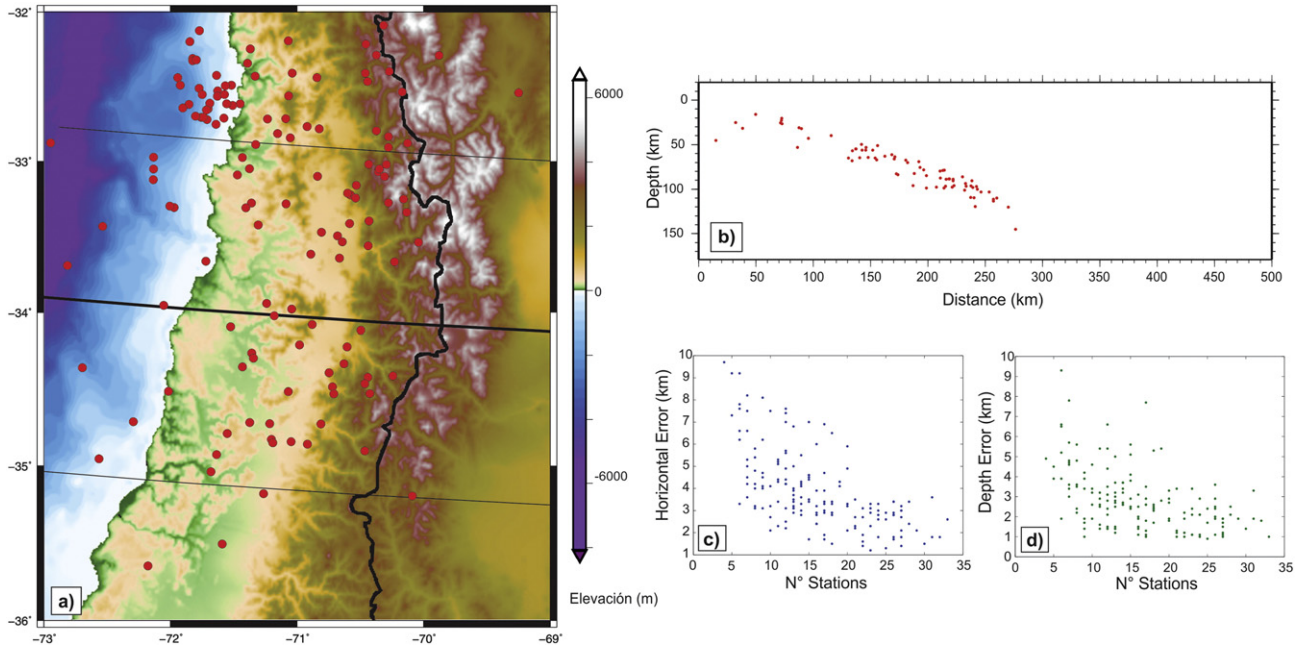

Fig. 4. Final results from GMEL with their respective errors. a) Epicenters selected after different quality test. The thick black line indicates the cross-section location plot in b) and the two thin black lines enclose the selected epicenters to be plotted in the cross-section. b) Cross-section shows the hypocenters in the interest zone. c) The horizontal error (semi-major axis of error ellipse) and the d) vertical error (semi-confidence depth interval) are plotted against stations used in the locations.

independent and that each is sampled from a generalized Gaussian or power exponential probability distribution (Rodi, 2006).

4. Results

A comparison between Hypocenter and GMEL location results is shown in Fig. 3. In general when the seismic events are located outside the experiment covered area the results from the different methods show marked differences. Conversely, after running GMEL the scatter in depth was diminished, if the results are compared with HYPOCENTER locations.

After applying different tests to the data a new subset was selected for relocation considering the confidence region of event location and weighted residual norm (wrn). The selection criterion was semi-major axis of error ellipse <20 km (horizontal error), semi-confidence interval <20 km (vertical error) and wrn <0.5 s. The final results shown for 157 Nazca plate events (Fig. 4 and Table 1 in Appendix) have less scattered solutions with uncertainties in the horizontal and vertical less than ±8 km (only 5 quakes have errors between ±10 km and ±8 km). When the station number is greater than 20 it is noticeable the decreasing of the horizontal and vertical error (Fig. 4c and 4d). The better results from a point of view of weighted residual norm were obtained considering that data errors follow the Laplace distribution (two-sided exponential). The focal depth is the location parameter with the least constraint, considering that rays are mainly upward (in local earthquakes). In addition to the error analysis in Fig. 4, the depth error for each earthquake (earthquakes which are enclosed within the thin black lines in Fig. 4a) is shown with vertical error bars (Fig. 5a). The lower to the epicentral distance to the nearest station, the greater will be control (in part) in the focal depth. The 75% of the earthquakes have at least one station at epicentral distance between 2.5 km and 50 km, showing depth uncertainties between ±0.9 km and ±5.1 km (Fig. 5b). However the low number of stations seems to be controlling the depth error in those earthquakes which have presented the greater errors (see the 3 earthquakes with depth errors between 6.5 km and 9.3 km in Fig. 5c).

Focal mechanism solutions were obtained from the first P motion for the located events using HASH code (Hardebeck and Shearer, 2002). This method takes into account possible errors in the assumed earthquake locations, uncertainties refer to the velocity model with the possibility of using different velocity models and uncertainties in the polarity observations. We performed a grid search over the strike, dip and rake using an angle of 5° to find a set of acceptable solutions (after averaging them to find a preferred solution) following the flowchart shown in Fig. 8 of Hardebeck and Shearer (2002). The results (Fig. 6 and Table 2 in Appendix) do not show a dominant type of focal mechanisms, but rather denote variability in their solutions.

5. Discussion

We plotted the aftershocks (violet points in Fig. 7a) of Mw 8.0 March 3, 1985 Valparaiso earthquake to map the interface zone in the study region. From those events and the marked change in number of seismic events located in this work (red points in Fig. 7a) we propose the downdip edge of the seismogenic interface zone at ~47–50 km depth. In a global study (Heuret et al., 2011) in which it is assumed that the seismogenic zone coincides with the distribution of shallow (depth ≤ 70 km) and moderately sized (5.5 ≤ Mw < 7.0) thrust fault earthquakes, a great variability of the downdip limit of the interface zone is observed, encompassed between 30 and 66 km. In particular, for the study region, Pardo et al. (2002) suggested the maximum

Fig. 3. Results from HYPOCENTER (blue circles) and GMEL (red circles) locations, the thin black line links the two results for the same event. a) Epicenters from the Nazca oceanic plate, the black thick line shows where the cross-section is located. The eastern epicenters north to 32.5° correspond to the Nazca flat slab section. The inset plot shows the 1-dimensional P velocity model used in this work from Nacif (2012). b) Cross-section shows the hypocenters for map in a), the eastern epicenters correspond to the flat slab section.

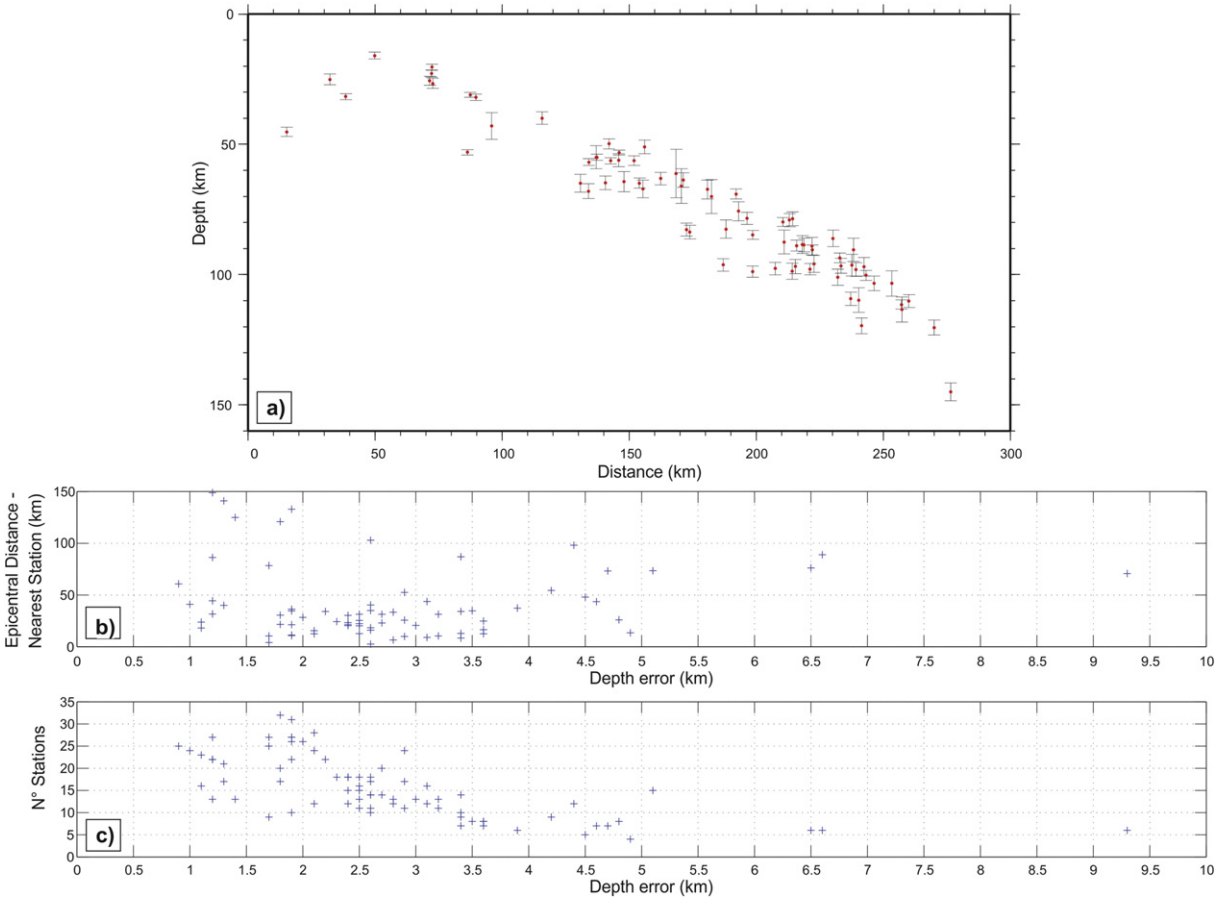

Fig. 5. Depth error analysis for the 76 earthquakes which are enclosed within the thin black lines in Fig. 4a). a) Cross-section plotted using the same origin, azimuth and profile width as those in Fig. 4. The red points show the hypocenters and the black bars their depth error (uncertainties). b) The epicentral distances for the nearest station are plotted against the depth errors. c) The numbers of stations used in each earthquake locations are plotted against their depth errors.

depth of the interface coupling at 51 km. Oleskevich et al. (1999) located the downdip limit range between 47 and 50 km depth for a cross-section at Valparaiso latitude from 2D thermal and structural models.

At least for the CHASE Experiment period and between 33° and 35°S we observed that the interface zone is poor in seismic activity (between ~10 and 50 km), below the interface zone between 50 and 120 km depth the Nazca plate becomes more seismically active and beneath ~120 km depth only one event is observed, according to Marot (2013) results. Using high resolution thermal models and improved petrological modeling van Keken et al. (2011) obtained a global dehydration of slabs as function of depth in subduction zones. From their Fig. 6 (which is a plot of water loss as function of depth in different subduction zones) we extracted the predicted water loss for Central Chile and it was plotted in our Fig. 7c. We observed that the range of slab water loss goes from ~70 km to 110 km depth, from ~160 km to 230 km depth and between ~110 km and 150 km there is no slab water loss observed. Basically our results are consistent with van Keken et al (2011) models and based on this the seismicity located between 70 and 120 km is probably related with dehydration processes (e.g., Kirby et al., 1996) rather than mechanical processes.

From precise locations below the interface zone we could approximate the slab dip angle to 27° in respect to the horizontal. This same value is obtained by other researchers (Pardo et al., 2002; Anderson et al., 2007) from other Seismological Experiments. An important contribution of this research is the complete lack of intraslab seismicity below 120 km depth. In subduction zones the maximum depth of seismic events is principally governed by temperature and pressure (Gorbatov and Kostoglodov, 1997). So this valuable finding can be used to better constrain thermal models for the region under study. From International Catalog (NEIC-USGS) and from EHB Bulletin (see cross-sections at latitudes 33.5°S and 34.5°S shown in Fig. 2) seismicity decreases below ~135 km depth, beneath from that depth the seismicity becomes scattered. Additionally, at those same latitudes, below ~100 km depth, a fringe of normal focal mechanism solutions (in general Mw > 5.0) was identified which could be related to the slab pull forces (see inset in Fig. 7a) and/or outer rise normal fault reactivation. However from a Southern Andes Seismological Experiment between 36° and 40°S latitude (Bohm et al., 2002) and from other regional experiment (east–west transect at 35° and 36°S), the intraslab seismicity continues up to depth of 150–200 km. Bohm et al. (2002) observed decreasing seismicity from north to south which they explained as a consequence of thermal structure change of the subducting oceanic plate. In this way, south of 39°S almost there are no earthquakes occurring in the young and hot oceanic lithosphere. The slab age increases to the north so it is expected to find deeper events at latitudes between 33° and 35°S compared with the results found by Bohm et al. (2002) and Anderson et al. (2007) for more southern zone. The last is not observed, we attribute this effect in part to the complex study zone (part of the transition subduction zone) in this work which must be affected by the flat slab shape north of 33°S. Also the absence of seismic events below 120 km depth is in accordance with the lack of a dehydration mechanism available to produce this seismicity, considering slab

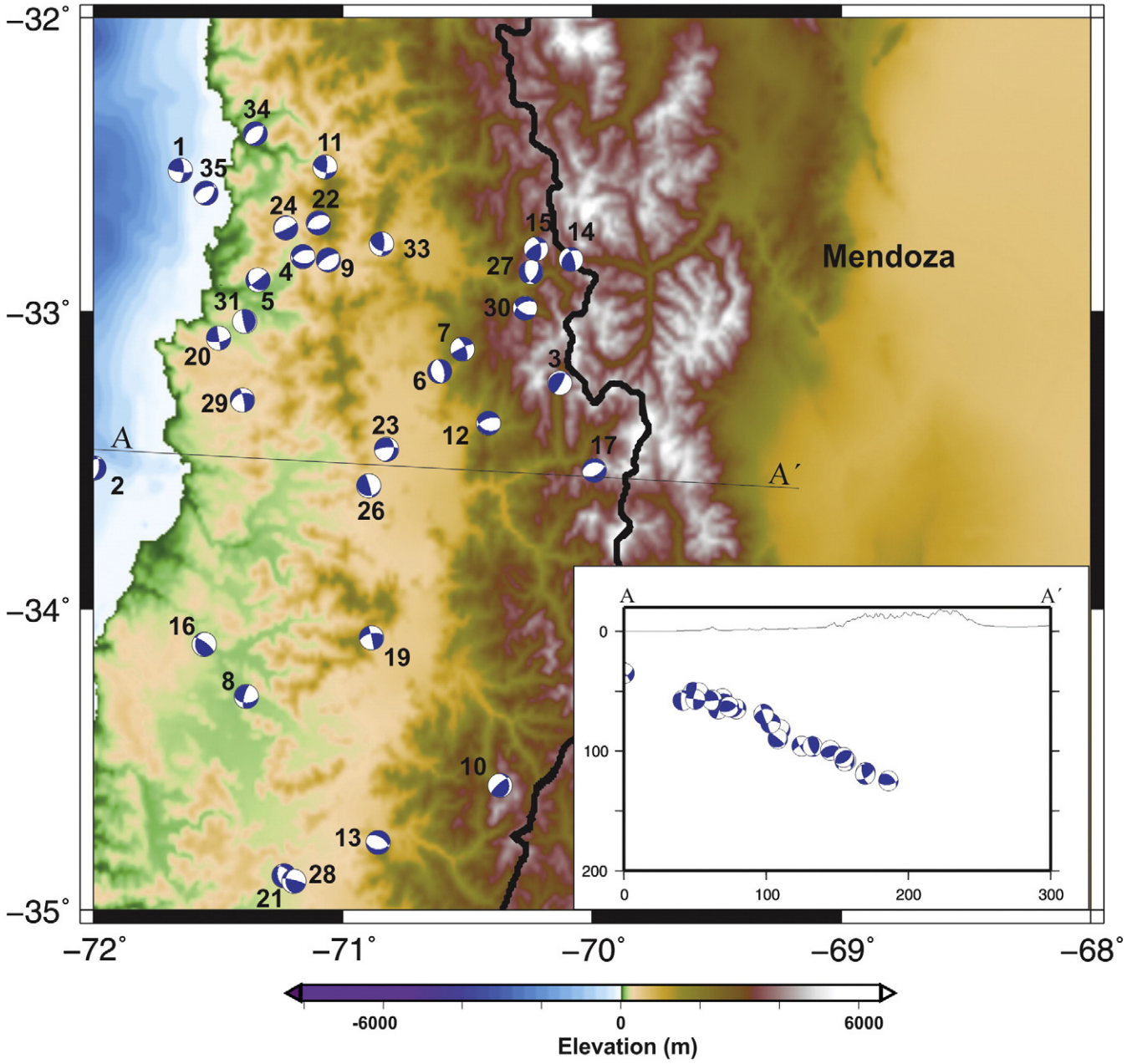

Fig. 6. Focal mechanism solutions from P-first motion using HASH code. The number near each mechanism is the identification number (IN), see Table 2 from Appendix. There are noticeable variations in the focal mechanism solutions. The most common solution type is the normal solution and a minor part is thrust and strike slip solutions.

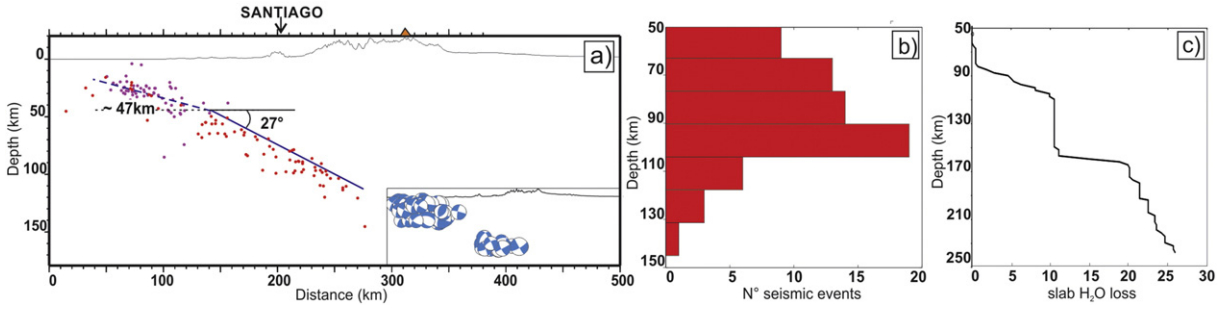

Fig. 7. a) Cross-section which shows the seismicity located in this work (red points) and the aftershocks EHB Catalog (Engdahl and Villaseñor, 2002) of Mw 8.0, March 3, 1985 Valparaiso earthquake for a period of 10 months after the principal earthquake (violet points). Downdip edge proposes located at ~47–50 km depth and the slab dip below this limit of 27°. The inset shows the focal mechanism solutions from CMT Catalog (http://www.globalcmt.org/CMTsearch.html), notice there is a gap of seismic events with Mw > 5.0. b) Number of seismic events below the interface zone as function of depth. Most of the intraslab earthquakes located between ~60 km and 105 km depth. c) Predicted water loss for central Chile extracted from Fig. 6 of van Keken et al. (2011).

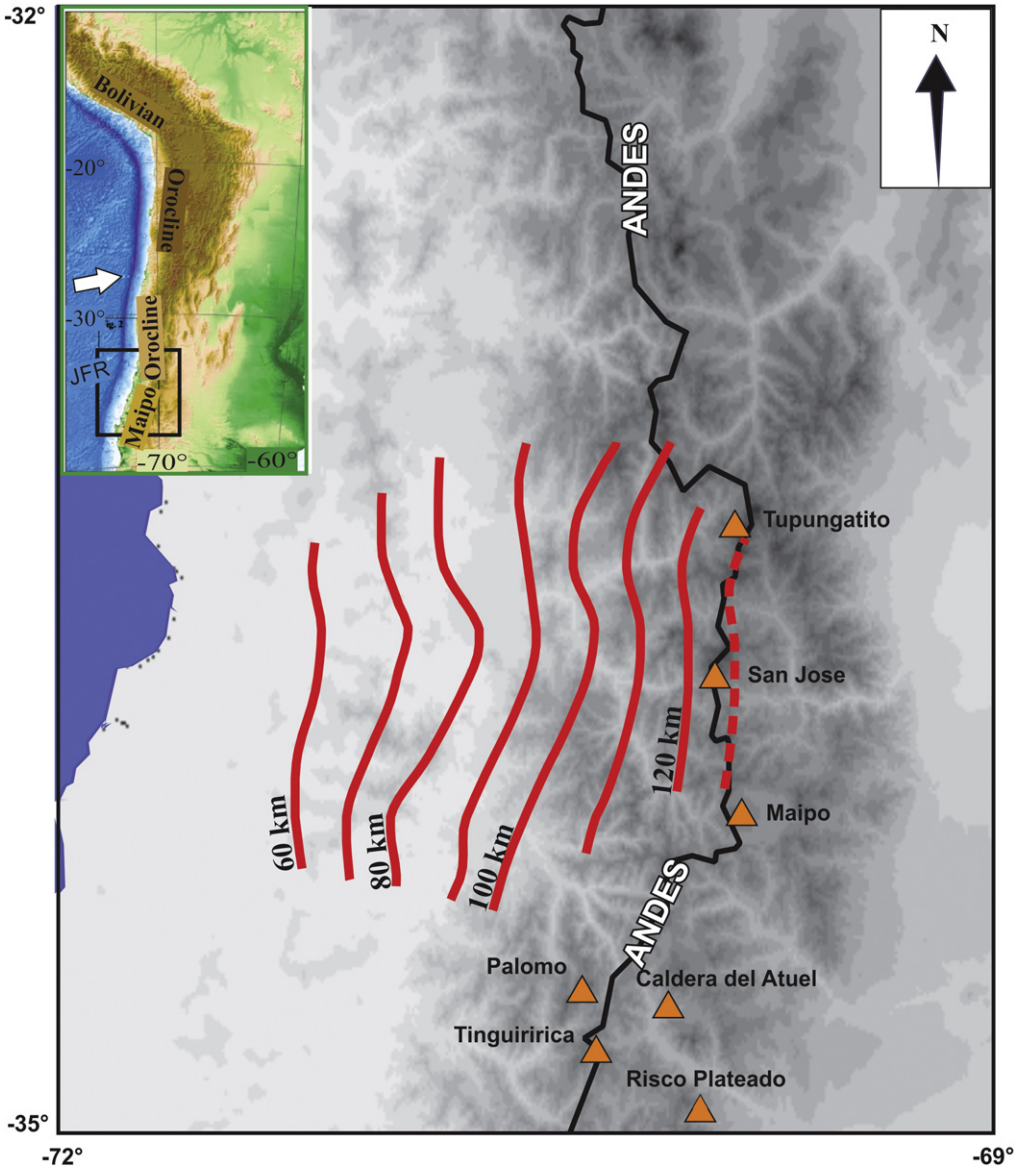

Fig. 8. Morphology of the Nazca subducted plate obtained in this work. Software blockmean, surface and grdcontour from GMT (The Generic Mapping Tools, http://gmt.soest.hawaii.edu/) were used. Only the constrained part of the slab contours is shown, considering the station coverage and the seismicity density. The upper left box (taken and modified from Arriagada et al. (2013)) shows the study region (black box) related with Maipo Orocline. The white arrow shows convergence subduction direction.

water loss model (van Keken et al., 2011) which predicts that between 110 km and 150 km depth there is no dehydration process in the subducted slab.

Slab contours below seismogenic interface zone were recovered in this work between 33° and 34.5°S (Fig. 8) from seismic events shown in Fig. 4. At these latitudes the oceanic trench, the continental border and the cordillera show a curvature (concave to the ocean), also a similar shape is observed in the morphology of the Nazca plate obtained in this work. In Central Andes, since 10–15 Ma Juan Fernández Ridge has been subducting continuously and could be the principal cause for Maipo Orocline (Arriagada et al., 2013). We propose that the subducting plate was deformed at the trench consistently with Maipo Orocline and this feature is still observed (below the interface zone) in the shape of the subducted plate (see Fig. 8). Furthermore, Fig. 8 shows the new active volcanic arc represented by Tupungatito, San Jose and Maipo volcanoes, outcrop where the subducted slab reaches the 130 km in the transition to low seismicity.

If dehydration embrittlement processes facilitate intraslab seismicity this seismicity could be partially responsible for promoting the volcanism above the subducted plate. From Fig. 7, it is evident that the volcanoes appear only in the transition to low seismicity. We interpreted that if the dehydration process produces the intraslab seismicity then the water lost in a range of ~70–100 km remains on the top of the subducted plate (e.g., Castro et al., 2010) and it is not transported out of the plate. This water is transported down to deeper levels where the diminishing of seismic events could evidence some kind of physical change in the plate. The water lost below ~100 km depth is consistent with tomographic results for a cross-section at 34°S (Wagner et al., 2005) which allow illuminating the mantle wedge above the subducting slab. Low Vp (P wave velocity), low Vs (S wave velocity) and high Vp/Vs are characteristics of partial melting (e.g., Nakajima et al., 2001; Zhang et al, 2004) or mantle wedge serpentinization (e.g., Hyndman and Peacock, 2003; Matsubara et al., 2009). The serpentine stability field is generally stable at temperatures beneath 700 °C (Bose and Ganguly, 1995; Hacker et al., 2003). Synthetic thermal model (at 33.5°S) manifests that the temperature in the mantle wedge zone is higher than 700° (Marot, 2013) and serpentine is not stable at such high temperatures. Wagner et al. (2005) found a high Vp/Vs (at 70°W) relation and associated with localized pockets of melt, probably induced by introduction of water into the mantle by the subducting slab. We suggest

that in the transition to low seismicity (between ~120 and 130 km) the water from the dehydration process (transport water from 70 to 120 km) is released and transported out of the subducted plate to produce the partial melt in mantle wedge which promotes the volcanism above.

6. Conclusions

From this work a constrained data set which describes the upper Nazca plate boundary between 33° and 34.5°S from ~47–50 km to 120 km depth was obtained. The down dip edge proposed at ~47–50 km is consistent with the aftershock distribution of the Mw 8.0 March 3, 1985 Valparaiso earthquake and with the thrust focal mechanisms (Mw > 5.0) generated in seismogenic interface zone. We suggest as a possible interpretation that the intraslab seismicity between depths of 70 and 120 km, could be favored and/or originated by dehydration reactions in the Nazca plate rather than mechanical processes. This in light of van Keken et al. (2011) predicted water loss model for the subduction zone of Central Chile. The abrupt seismicity finalization at 120 km depth founded in this research could be used to better constrain thermal models for the region. The noticeable similarity between the subducted plate mapped by contours obtained in this work (beneath the interface zone) and the Maipo Orocline reveals some strong connection between both lithospheres. We advise that the subducted plate at the trench has been deformed consistently with the Maipo Orocline and its deformation remains and is observed below the interface zone. Also in the transition to low seismicity (at ~120–130 km depths), we propose that the water from the dehydration process (transport water from 70 to 120 km) is released and transported out of the subducted Nazca plate to produce the partial melt in the mantle wedge which promotes the volcanism above.

Acknowledgments

This material is based on work supported by CHile Argentina Seismic Experiment developed by the project "*Crustal seismicity and velocity structure in the principal cordillera of central Chile 33°–34.5°S: implications on Andean geodynamic and seismic hazard*", FONDECYT 1050758, Chile, Director: Dr. Mario Pardo. Many thanks to William Rodi for allowing us to use his grid multiple events location code GMEL and assistance in using it. The authors would like to thank the CONICET (Consejo Nacional de Investigaciones Científicas y Técnicas) for financial support. A special acknowledgement is given to Dr. Vlad Manea one of the reviewers and to the other unknown reviewer. In addition a gratitude is given to Dr. Peter van Keken who kindly provided a figure which has allowed us to make important interpretations.

Appendix A. Supplementary data

Supplementary data to this article can be found online at http://dx.doi.org/10.1016/j.tecto.2015.06.027.

References

Anderson, M.L., Alvarado, P., Zandt, G., Beck, S., 2007. Geometry and brittle deformation of the subducting Nazca Plate, Central Chile and Argentina. Geophys. J. Int. 171 (1), 419–434.

Araujo, M., Suarez, G., 1994. Geometry and state of stress of the subducted Nazca plate beneath central Chile and Argentina: evidence from teleseismic data. Geophys. J. Int. 116 (2), 283–303.

Arriagada, C., Ferrando, R., Córdova, L., Morata, D., Roperch, P., 2013. The Maipo Orocline: a first scale structural feature in the Miocene to Recent geodynamic evolution in the central Chilean Andes. Andean Geol. 40 (3), 419–437.

Barcheck, C., Wiens, D., vanKeken, P., Hacker, B., 2012. The relationship of intermediate- and deep-focus seismicity to the hydration and dehydration of subducting slabs. Earth Planet. Sci. Lett. (349–350), 153–160.

Barrientos, S.E., 1988. Slip distribution of the 1985 central Chile earthquake. Tectonophysics 145 (3-4), 225–241.

Bengston, A.K., van Keken, P.E., 2012. Three-dimensional thermal structure of subduction zones: effects of obliquity and curvature. Solid Earth 3, 365–373.

Bohm, M., Lüth, S., Echtler, H., Asch, G., Bataille, K., Bruhn, C., Rietbrock, A., Wigger, P., 2002. The Southern Andes between 36° and 40°S latitude: seismicity and average seismic velocities. Tectonophysics 356 (4), 275–289.

Bose, K., Ganguly, J., 1995. Experimental and theoretical studies of the stabilities of talc, antigorite and phase A at high pressures with applications to subduction processes. Earth Planet. Sci. Lett. 136, 109–121.

Braeck, S., Podladchikov, Y.Y., 2007. Spontaneous thermal runaway as an ultimate failure mechanism of materials. Phys. Rev. Lett. 98, 095504.

Cahill, T., Isacks, B.L., 1992. Seismicity and shape of the subducted Nazca plate. J. Geophys. Res. 97 (B12), 17503–17529.

Castro, A., Gerya, T.V., Garcia-Casco, A., Fernández, C., Díaz-Alvarado, J., Moreno-Ventas, I., Löw, I., 2010. Melting relations of MORB-sediment mélanges in underplated mantle wedge plumes; implications for the origin of Cordilleran-type batholiths. J. Petrol. 51 (6), 1267–1295.

Choy, G.L., Dewey, J.W., 1988. Rupture process of an extended earthquake sequence: teleseismic analysis of the Chilean earthquake of March 3, 1985. J. Geophys. Res. 93 (B2), 1103–1118.

Christensen, D., Ruff, L., 1986. Rupture process of the March 3, 1985 Chilean earthquake. Geophys. Res. Lett. 13 (8), 721–724.

Comte, D., Eisemberg, A., Lorca, E., Pardo, M., Ponce, L., Saragoni, R., Singh, S.K., Suarez, G., 1986. The 1985 central Chile earthquake: a repeat of previous great earthquakes in the region? Science 233, 449–453.

Crotwell, H.P., Owens, T.J., 1998. The TauP Toolkit: Flexible Seismic Travel-Time and Raypath Utilities Version 2.0. Department of Geological Sciences, University of South Carolina.

Engdahl, E.R., Villaseñor, A., 2002. Global seismicity: 1900–1999. In: Lee, W.H.K., Kanamori, H., Jennings, P.C., Kisslinger, C. (Eds.), International Handbook of Earthquake and Engineering Seismology. Academic Press, pp. 665–690 (Part A, Chapter 41).

England, P., Engdahl, R., Thatcher, W., 2004. Systematic variation in the depths of slabs beneath arc volcanoes. Geophys. J. Int. 156 (2), 377–408.

Farías, M., Charrier, R., Carretier, S., Martinod, J., Fock, A., Campbell, D., Cáceres, J., Comte, D., 2008. Late Miocene high and rapid surface uplift and its erosional response in the Andes of Central Chile (33°–35°S). Tectonics 27 (1). http://dx.doi.org/10.1029/2006TC002046.

Gerya, T., Fossati, D., Cantieni, C., Seward, D., 2009. Dynamic effects of aseismic ridge subduction: numerical modelling. Eur. J. Mineral. 21, 649–661.

Gorbatov, A., Kostoglodov, V., 1997. Maximum depth of seismicity and thermal parameter of the subducting slab: general empirical relation and its application. Tectonophysics 277, 165–187.

Gutscher, M.A., Spakman, W., Bijwaard, H., Engdahl, E.R., 2000. Geodynamics of flat subduction: seismicity and tomographic constraints from the Andean margin. Tectonics 19 (15), 814–833.

Hacker, B.R., Peacock, S.M., Abers, G.A., Holloway, S.D., 2003. Subduction factory 2. Are intermediate-depth earthquakes in subducting slabs linked to metamorphic dehydration reactions? J. Geophys. Res. 108 (B1). http://dx.doi.org/10.1029/2001JB001129.

Hardebeck, J., Shearer, P., 2002. A new method for determining first motion focal mechanisms. Bull. Seismol. Soc. Am. 92 (6), 2264–2276.

Havskov, J., Ottemöller, L., Canabrava, R.L.P., 2007. SEISAN: multiplatform implementation of MINISEED/SEED. Orfeus Newsletter 7 (2).

Hayes, G., Wald, D., 2009. Advancing techniques to constrain the geometry of the seismic rupture plane on subduction interfaces a priori: higher-order functional fits. Geochem. Geophys. Geosyst. 10 (9). http://dx.doi.org/10.1029/2009GC002633.

Hayes, G., Wald, D., Johnson, R., 2012. Slab1.0: a three-dimensional model of global subduction zone geometries. J. Geophys. Res. 117 (B01302). http://dx.doi.org/10.1029/2011JB008524.

Heuret, A., Lallemand, S., Funiciello, F., Piromallo, C., Faccenna, C., 2011. Physical characteristics of subduction interface type seismogenic zones revisited. Geochem. Geophys. Geosyst. 12 (1). http://dx.doi.org/10.1029/2010GC003230.

Hildreth, W., Moorbath, S., 1988. Crustal contributions to arc magmatism in the Andes of Central Chile. Contrib. Mineral. Petrol. 98 (4), 455–489.

Hyndman, R., Peacock, S., 2003. Serpentinization of the forearc mantle. Earth Planet. Sci. Lett. 212, 417–432.

Jiao, W., Silver, P.G., Fei, Y., Prewitt, C.T., 2000. Do intermediate- and deep-focus earthquakes occur on pre-existing weak zones? An examination of the Tonga subduction zone. J. Geophys. Res. 105 (B12), 28125–28138.

John, T., Medvedev, S., Rüpke, L.H., Andersen, T.B., Podladchikov, Y.Y., Austrheim, H., 2009. Generation of intermediate-depth earthquakes by self-localizing thermal runaway. Nat. Geosci. 2, 137–140.

Jung, H., Green, H.W., Dobrzhinetskaya, L.W., 2004. Intermediate-depth earthquake faulting by dehydration embrittlement with negative volume change. Nature 428, 545–549.

Kay, S.M., Maksaev, V., Moscoso, R., Mpodozis, C., Nasi, C., 1987. Probing the evolving Andean Lithosphere: Mid-late Tertiary magmatism rocks in Chile (29°–30°30′S) over the modern zone of subhorizontal subduction. J. Geophys. Res. 92 (B7), 6173–6189.

Kay, S., Godoy, E., Kurtz, A., 2005. Episodic arc migration, crustal thickening, subduction erosion, and magmatism in the south-central Andes. GSA Bull. 117 (1-2), 67–88.

Kelemen, P.B., Hirth, G., 2007. A periodic shear-heating mechanism for intermediate-depth earthquakes in the mantle. Nature 446, 787–790.

Kendrick, E., Bevis, M., Smalley, R.J., Brooks, B.A., Barriga, R., Lauría, E., Souto, L.P., 2003. The Nazca–South America Euler vector and its rate of change. J. S. Am. Earth Sci. 16 (2), 125–131.

Kirby, S., Engdalh, E.R., Denlinger, R., 1996. Intermediate-depth intraslab earthquake and arc volcanism as physical expressions of crustal and uppermost mantle metamorphism in subducting slabs. In: Bebout, G.E., School, D.W., Kirby, S.H., Platt, J.P.

(Eds.), Subduction Top to Botton: American Geophysical Union Geophysical Monograph 96, pp. 195–214.
Klein, F.W., 2002. Hypocenter Location Program HYPOINVERSE. US Geological Survey Open File Reportpp. 02–171 (Version 1.0.).
Liener, B.R., Havskov, J., 1995. A computer program for locating earthquakes locally, regionally and globally. Seismol. Res. Lett. 66, 26–36.
Manea, V.C., Gurnis, M., 2007. Subduction zone evolution and low viscosity wedges and channels. Earth Planet. Sci. Lett. 264, 22–45.
Manea, V.C., Pérez-Gussinyé, M., Marina, Manea M., 2012. Chilean flat slab subduction controlled by overriding plate thickness and trench rollback. Geology 40, 35–38.
Marot, M., 2013. Flat versus normal subduction zones: a comparison based on 3-D regional travel-time tomography and petrological modeling of central Chile and western Argentina (29°–35°S) Dr. Thesis, Université de Nice-Sophia Antipolis - UFR Sciences, France (224 pp. (in English)).
Marot, M., Monfret, T., Pardo, M., Ranalli, G., Nolet, G., 2012. An intermediate-depth tensional earthquake (M_W 5.7) and its aftershocks within the Nazca slab, central Chile: a reactivated outer rise fault? Earth Planet. Sci. Lett. (327–328), 9–16.
Marot, M., Monfret, T., Gerbault, M., Nolet, G., Ranalli, G., Pardo, M., 2014. Flat vs. normal subduction zones: a comparison based on 3D regional traveltime tomography and petrological modeling of central Chile and western Argentina (29–35S). Geophys. J. Int. 199, 1633–1654.
Martinod, J., Funiciello, F., Faccenna, C., Regard, V., 2005. Dynamical effects of subducting ridges: insights from 3-D laboratory models. Geophys. J. Int. 163, 1137–1150.
Matsubara, M., Obara, K., Kasahara, K., 2009. High-VP/VS zone accompanying nonvolcanic tremors and slow-slip events. Tectonophysics 472 (1-4), 6–17.
Maurer, V., Kissling, E., Husen, S., Quintero, R., 2010. Detection of systematic errors in travel-time data using a minimum 1D model: application to Costa Rica seismic tomography. Bull. Seismol. Soc. Am. 100 (2), 629–639.
Meade, C., Jeanloz, R., 1991. Deep focus earthquakes and recycling of water into the Earth's mantle. Science 252, 68–72.
Mendoza, C., Hartzell, S., Monfret, T., 1994. Wide-band analysis of the 3 March 1985 central Chile earthquake: overall source process and rupture history. Bull. Seismol. Soc. Am. 84 (2), 269–283.
Nacif, S., 2012. Seismotectonic of the Nazca plate between 33°S and 35°S below the interplate seismogenic zone and seismic anisotropy in the crust and the upper mantle of the overriding plate Dr. Thesis, San Juan University, Argentina (217 pp. (in Spanish)).
Nakajima, J., Matsuzawa, T., Hasegawa, A., 2001. Three-dimensional structure of Vp, Vs, and Vp/Vs beneath northeastern Japan: implications for arc magmatism and fluids. J. Geophys. Res. 106, 21843–21857.
Nishenko, S., 1985. Seismic potential for large and great interplate earthquakes along the Chilean and southern Peruvian Margins of South America: a quantitative reappraisal. J. Geophys. Res. 90 (5), 3589–3615.
Ogawa, M., 1987. Shear instability in a viscoelastic material as the cause of deep focus earthquakes. J. Geophys. Res. 92 (B13), 13.801–13.810.
Oleskevich, D.A., Hyndman, R.D., Wang, K., 1999. The updip and downdip limits to great subduction earthquakes: thermal and structural models of Cascadia, south Alaska, SW Japan, and Chile. J. Geophys. Res. 104 (B7), 14965–14991.
Pacheco, J.F., Sikes, L.R., Scholz, C.H., 1993. Nature of seismic coupling along simple plate boundaries of the subduction type. J. Geophys. Res. 98 (B8), 14133–14159.
Pardo, M., Comte, D., Monfret, T., 2002. Seismotectonic and stress distribution in the central Chile subduction zone. J. S. Am. Earth Sci. 15 (1), 11–22.
Raleigh, C.B., Paterson, M.S., 1965. Experimental deformation of serpentinite and its tectonic implications. J. Geophys. Res. 70 (16), 3965–3985.
Rodi, W., 2006. Grid-search event location with non-Gaussian error models. Phys. Earth Planet. Inter. 158, 55–66.
Ruff, L., Kanamori, H., 1983. Seismic coupling and uncoupling at subduction zones. Tectonophysics 99 (2–4), 99–117.
Ruff, L., Tichelaar, B., 1996. What controls the seismogenic plate interface in subuction zones. In: Bebout, G.E., School, D.W., Kirby, S.H., Platt, J.P. (Eds.), Subduction Top to Bottom. American Geophysical Union Geophysical Monograph 96, pp. 105–111.
Syracuse, E.M., Abers, G.A., 2006. Global compilation of variations in slab depth beneath arc volcanoes and implications. Geochem. Geophys. Geosyst. 7 (5). http://dx.doi.org/10.1029/2005GC001045.
Tichelaar, B.W., Ruff, L.J., 1991. Seismic coupling along the Chilean subduction zone. J. Geophys. Res. 96 (B7), 11997–12022.
van Hunen, J., van der Berg, A.P., Vlaar, N.J., 2002. On the role of subducting oceanic plateaus in the development of shallow flat subduction. Tectonophysics 352, 317–333.
van Hunen, J., van der Berg, A.P., Vlaar, N.J., 2004. Various mechanisms to induce present-day flat subduction and implications for the younger Earth: a numerical parameter study. Phys. Earth Planet. Inter. 146, 179–194.
van Keken, P.E., Hacker, B.R., Syracuse, E.M., Abers, G.A., 2011. Subduction factory 4: depth-dependent flux of H_2O from subducting slabs worldwide. J. Geophys. Res. 116 (B1). http://dx.doi.org/10.1029/2010JB007922.
Wagner, L.S., Beck, S., Zandt, G., 2005. Upper mantle structure in the south central Chilean subduction zone (30° to 36°S). J. Geophys. Res. 110 (B1). http://dx.doi.org/10.1029/2004JB003238.
Yáñez, G., Cembrano, J., Pardo, M., Ranero, C., Selles, D., 2002. The Challenger–Juan Fernandez–Maipo major tectonic transition of the Nazca–Andean subduction system at 33–34°S: geodynamics evidence and implications. J. S. Am. Earth Sci. 15, 23–38.
Zhang, H., Thurber, C., Shelly, D., Ide, S., Beroza, G., Hasegawa, A., 2004. High-resolution subducting-slab structure beneath northern Honshu, Japan, revealed by double-difference tomography. Geology 32 (4), 361–364.